Acta Cryst. (1979). A35, 38–44

Contribution of Diffraction to the Contrast of Dislocations in X-ray Topography*

BY Y. EPELBOIN†

IBM T. J. Watson Center, PO Box 218, *Yorktown Heights, NY* 10598, *USA*

(*Received* 24 *March* 1978; *accepted* 10 *July* 1978)

Abstract

The influence of both diffraction and geometrical optics in the formation of the contrast of dislocations in X-ray topography has been studied; it is shown that newly created wavefields, *i.e.* diffraction, are mainly responsible for the contrast of such a defect except in the case of a minimum of contrast which may be explained by geometrical optics only. It is concluded that it is not possible in general to determine the sense of the Burgers vector of a dislocation with geometrical theories alone and that diffraction must be taken into account.

Introduction

The contrast of dislocations in X-ray projection topographs is now well understood; it is usual to distinguish three parts in the image of a defect: the direct image which may be approximately explained through kinematical diffraction and the intermediary and dynamical images which are due to dynamical phenomena. The main achievement was when Balibar & Authier (1967) were able to simulate the complete image of a dislocation by the means of a computer. This also proved that the equations established by Takagi (1962, 1969) and Taupin (1964) successfully predict the contrast of any kind of defect. The disadvantage is that the notion of wavefields disappears and that simulations give only a global understanding without any exact knowledge and satisfactory explanation for the contrast of the defect. It is not possible to appreciate exactly what happens in the deformed part of the crystal.

The contrast of deformed crystals may be also studied by theories based on geometrical optics (Penning & Polder, 1961; Kato, 1963); their main advantage is that the notion of wavefields is not lost and that it is possible to calculate their paths. Using this theory Kambe (1963) came to the conclusion that the dynamical image is the caustic of wavefields bent by the deformed areas near the dislocation. Unfortunately this theory is limited with respect to large deformations and it was necessary to neglect the contribution of areas near the core where strains are very large. It is particularly well known that the intermediary image may not be explained through the Eikonal theory (Authier, 1967) and that observed fringes are the result of interferences between normal and extra wavefields. This has led to the concept of newly created wavefields (Authier & Balibar, 1970) and has been proved experimentally (Authier, Balibar & Epelboin, 1970).

The contrast of a dislocation may thus be explained taking into account both phenomena: the curved wavefields of the Eikonal theory which correspond to the geometrical optics and the newly created wavefields which are a diffraction phenomenon.

In this paper we try to understand the relative importance of these phenomena in the formation of the contrast of a dislocation. We first recall the meaning of the criterion of the geometrical optics which separates the domains of validity of the theories which deal with geometrical optics or diffraction; we then apply it to the study of the contrast of different dislocations. This is done by means of computer simulations.

I. Geometrical optics and diffraction

The physical explanation of both phenomena may be understood through the notion of wave packets (Balibar & Malgrange, 1975; Balibar, 1975).

The Eikonal theory is based on the assumption that any wavefield may be considered as the sum of individual plane waves. When a deformation exists somewhere in the crystal a plane wave remains a plane wave; its path is bent but it is possible to follow each individual wavefield through the whole crystal.

Let us now consider a wave packet incident on the crystal in place of individual plane waves. We can no longer attribute a unique wave vector to the wave packet, which now possesses a certain extension $\Delta\mathbf{k}$ in reciprocal space. In the crystal, both wavefields corresponding to an incident plane wave must now be replaced by two 'subwave' packets of approximately

* This paper was presented, by invitation, at the ACA Dynamical Diffraction Symposium held at the University of Oklahoma, 22 March 1978, honoring Paul P. Ewald on the occasion of his ninetieth birthday.

† Permanent address: Laboratoire de Minéralogie–Cristallographie, associé au CNRS, Université P. M. Curie, 75230 Paris CEDEX 05, France.

0567-7394/79/010038-07$01.00

the same extension $\Delta\mathbf{k}$ which are separated by a distance of the order of the diameter of the dispersion surface, *i.e.* approximately $1/\Lambda$, where Λ is the extinction distance. As long as the lateral extension of the wavepacket is not too large each subwave packet retains its individuality and may be described as a Bloch wave. When the deformation of the crystal increases it may happen that both subwave packets overlap in reciprocal space, then the notion of wavefield is lost and beyond the deformed area new subwave packets will appear. These are newly created wavefields or, in other words, diffraction. The Eikonal theory corresponds to the case where a wave packet does not lose its structure composed of two subwave packets: diffraction phenomena may be neglected and it is simply a case of geometrical optics.

Crystal waves may be represented as modulated waves with a fast oscillation of periodicity λ, corresponding to the X-ray wavelength in the crystal modulated by a wave of periodicity Λ superimposed on it. The distortions inside the crystal do not affect the carrier wave itself since its oscillations are much faster than the variations of the local deformation but modify the modulation either by changing its length (geometrical optics) or when the deformation varies quickly by destroying the modulation itself (diffraction). The limit of validity of the geometrical optics may be predicted and this leads to the criterion of geometrical optics (Authier & Balibar, 1970).

Criterion of the geometrical optics

Let us write the well known Takagi–Taupin equations:

$$\partial^2 \psi_0/\partial \mathbf{s}_0\, \partial \mathbf{s}_h - 2i\pi k\beta'_h\, \partial\psi_0/\partial \mathbf{s}_0 + \pi^2 k^2 C^2 \chi_h \chi_{\bar{h}}\, \psi_0 = 0, \quad (1)$$

$$\partial^2 \psi_h/\partial \mathbf{s}_0\, \partial \mathbf{s}_h - 2i\pi k\beta'_h\, \partial\psi_h/\partial \mathbf{s}_0 + (\pi^2 k^2 C^2 \chi_h \chi_{\bar{h}} - 2i\pi k\, \partial\beta'_h/\partial \mathbf{s}_0)\, \psi_h = 0, \quad (2)$$

where $k = 1/\lambda$, χ_h and $\chi_{\bar{h}}$ are the Fourier components of the dielectric susceptibility, and $\mathbf{s}_0$ and $\mathbf{s}_h$ are unit vectors along the refracted and reflected directions respectively.

By an appropriate choice of the extremities of the wave vectors inside the crystal:

$$\beta'_h = (-1/k)\, \partial \mathbf{g}.\mathbf{u}(\mathbf{r})/\partial \mathbf{s}_h, \quad (3)$$

where $\mathbf{g}$ is the reciprocal-lattice vector corresponding to the reflection and $\mathbf{u}(\mathbf{r})$ the local deformation at point $\mathbf{r}$ inside the crystal.

Authier & Balibar (1970) have shown that Takagi's equations are equivalent to those established by Kato (1963) in the Eikonal theory when $\partial\beta'_h/\partial \mathbf{s}_0$ may be neglected in equation (2). If this is not the case, when $\pi^2 k^2 C^2 \chi_h \chi_{\bar{h}}$ becomes negligible in equation (2), the propagation of the waves inside the crystal may be described by diffraction optics. Thus, geometrical optics will be valid if:

$$2\pi k |\, \partial\beta'_h/\partial \mathbf{s}_0| \ll \pi^2 k^2 C^2 \chi_h \chi_{\bar{h}}. \quad (4)$$

This is the criterion of geometrical optics. We may write this as:

$$G \ll \tfrac{1}{2}.\pi k^2 C^2 \chi_h \chi_{\bar{h}}, \quad (5)$$

where $G = |\, \partial^2 \mathbf{g}.\mathbf{u}(\mathbf{r})/\partial \mathbf{s}_0\, \partial \mathbf{s}_h|$.

Balibar (1975) has shown that a wave packet will not lose its structure as long as this criterion is fulfilled. In other words, the Eikonal theory will be valid only if the radius of curvature of the net planes, near the defect, is much larger than Λ.

In a previous paper (Balibar, Epelboin & Malgrange, 1975), we studied the ratio of the diffracted wavefields as a function of G in a crystal deformed by a large thermal gradient. Increasing the gradient of deformation, we were able to change the value of G and we calculated the X-ray intensity on the exit surface of the crystal. It was possible to distinguish the diffracted wavefields from the curved ones and we plotted the diffracted intensity *versus* the values of G (Fig. 1).

We will apply these results to the understanding of the diffraction near the core of a dislocation line.

II. Diffraction effects in dislocation images

Deformations around the core of a dislocation are rather complicated and it is not possible to separate diffraction from geometrical optics. There is no way to modify G, as in the case of a thermal gradient, to give a predominant weight to one of these phenomena. Fig. 1 may be used to evaluate the amount of diffracted wavefield for a certain range of values for G. We see, for example, that if G is lower than a given value n only a certain percentage of the wavefields are diffracted. Thus if we modify the deformation around the core of the dislocation so that G is never greater than n, as shown schematically in Fig. 2(*a*), we will be able to understand the role of curved wavefields. On the other hand, if we only take into account the areas where G is greater than this cut-off value n (Fig. 2*b*) we will mostly study the contribution of the diffracted wavefields.

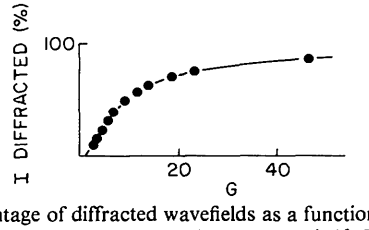

Fig. 1. Percentage of diffracted wavefields as a function of G in the case of a large thermal gradient. Unit: $\frac{1}{2}\pi k^2 C^2 \chi_h \chi_{\bar{h}}$ (after Balibar, Epelboin & Malgrange, 1975).

For this purpose we have modified a simulation routine (Epelboin, 1974, 1977); this calculates G at any point inside the crystal and, according to its value, allows one to take into account the areas where G is larger than a given cut-off value or to limit the deformation so that G is never larger than this cut-off value, following the rules described in Fig. 2. The complete simulation of the image of the defect is the reference and permits a determination of the importance of diffraction and geometrical optics.

(*a*) *Experimental data*

The dislocation under study has already been simulated (Balibar & Authier, 1967; Epelboin, 1974). It is inclined in a silicon wafer 800 μm thick; the reflection is Mo $K\alpha$ 220 in a symmetric setting.

We first consider the experimental case where $\mathbf{b} = \frac{1}{2}[\bar{1}0\bar{1}]$, thus $\mathbf{g}.\mathbf{b} \neq 0$; we then study a dislocation which presents a minimum of contrast with $\mathbf{g}.\mathbf{b} = 0$. In a second part we study the paths of the wavefields for an edge dislocation.

All simulations have been drawn by means of an IBM experimental printer (Handelmann, 1975).

(*b*) *Contrast when* $\mathbf{g}.\mathbf{b} \neq 0$

The dislocation is neither edge nor screw; the angle between the line and $\mathbf{b}$ is about 30°. Fig. 3 shows the contour map corresponding to the values of G around the core of the dislocation; it is drawn in a plane of incidence and the dislocation line crosses it in the middle of the square; its size is 10 × 10 μm. The contour line corresponding to the equality to the criterion of the geometrical optics $G = 1$ is outside Fig. 3 and extends to a distance of the order of 50 × 50 μm. According to Fig. 1, contour line 10 means that inside this line diffraction is predominant since more than 50% of the wavefields are diffracted. Fig. 4 shows the simulated projection topograph of this dislocation for various cut-off values for G. Fig. 4(*a*) is the reference since it includes all the deformed areas. The succeeding pairs of simulations are for $G \geq$ or $\leq n$, where n takes the values shown in Fig. 4(*b*)–(*g*). Some slight changes are noticeable in Fig. 4(*b*) which takes into account areas where $G \geq 1$ (the geometrical optics criterion). Fig. 4(*c*) is complementary: the simulation for $G \leq 1$ is unsatisfactory since only long-range stresses create this image. However, the differences between Fig. 4(*a*) which includes and 4(*b*) which neglects long-distance stresses show that their influence is important, especially in the dynamical image. This result demonstrates that X-ray topography is sensitive to long-range strain and that accurate simulations may not be obtained with the field of deformation limited. Figs. 4(*d*) and 4(*e*) correspond to a cut-off value $G = 10$; thus, in Fig. 4(*d*) diffraction is predominant since more than 50% of the wavefields are diffracted (Fig. 1). Although an important part of the deformation is suppressed the image is still good, much better than that obtained with predominance given to the curved wavefields as in the complementary simulation of Fig. 4(*e*), $G \leq 10$. Fig. 4(*f*) and 4(*g*) correspond to a cut-off value $G = 50$. The corresponding diffraction regions are very small as shown in Fig. 3, but Fig. 4(*f*) still retains the main feature of the whole image. Of course, Fig. 4(*g*) ($G \leq 50$) is better because the neglected areas are very small. These two last simulations clearly show the importance of diffraction contributing to the contrast. From the standpoint of geometrical optics Fig. 4(*e*), where G equals 10, may be considered as the limit of validity for any theory based on this phenomenon only; the simulated image is still very different from the complete one. Fig. 4(*f*), in which diffraction is predominant, bears much more resemblance to the reference Fig. 4(*a*). The conclusion is that diffraction may not be neglected if we wish to understand the contrast of dislocations for $\mathbf{g}.\mathbf{b} \neq 0$. Perhaps it is not

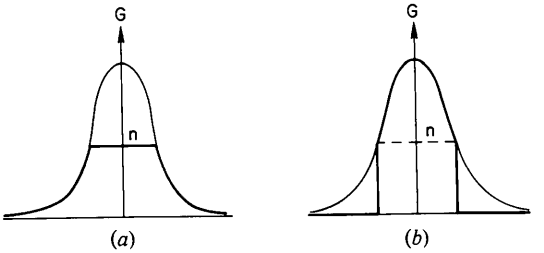

Fig. 2. Method of simulation. G values *versus* position of the current point along a line passing through the core of the dislocation. (*a*) Areas taken into account for G lower than the cut-off value n. (*b*) Areas taken into account for G greater than the cut-off value.

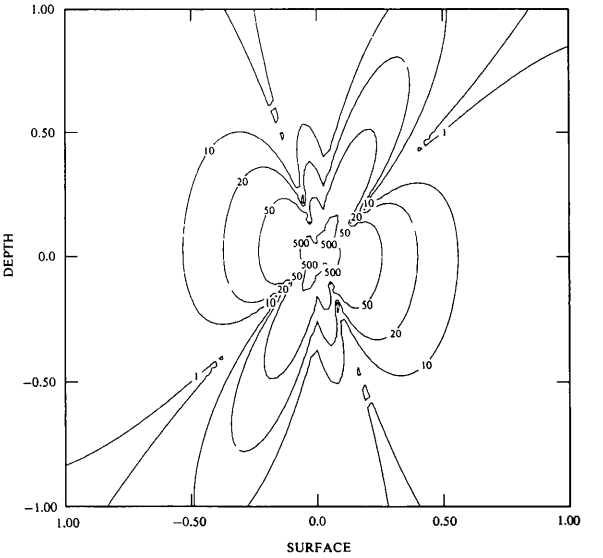

Fig. 3. Contour map for G in a plane of incidence (Mo $K\alpha$ 220, $\mathbf{b} = \frac{1}{2}[101]$, area 10 × 10 μm, unit as in Fig. 1).

too much of an exaggeration to say that the diffracted wavefields are the main phenomenon responsible for the contrast of such a dislocation.

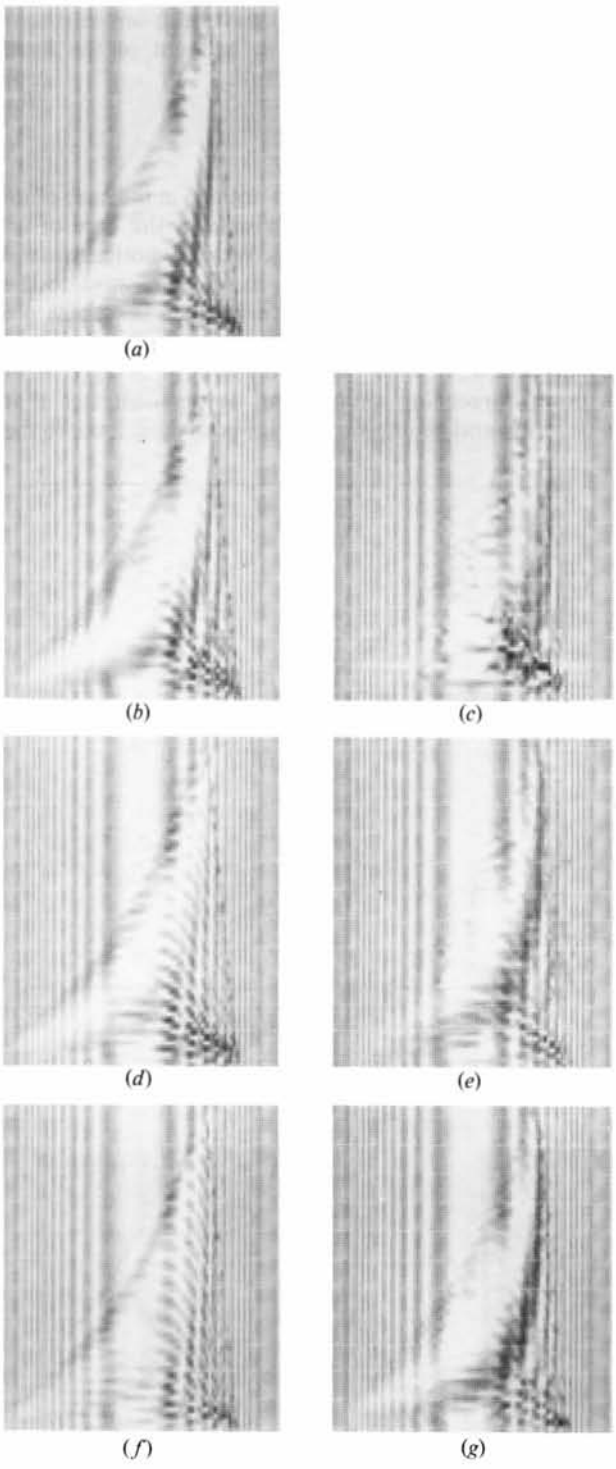

Fig. 4. Simulated projection topographs (conditions as in Fig. 3). (*a*) Complete simulation. (*b*) $G > 1$. (*c*) $G \leq 1$. (*d*) $G > 10$. (*e*) $G \leq 10$. (*f*) $G > 50$. (*g*) $G \leq 50$.

(*c*) *Contrast when* $\mathbf{g}.\mathbf{b} = 0$

Let us now consider a dislocation with the same orientation in the crystal but with a different Burgers vector $\mathbf{b} = \frac{1}{2}[1\bar{1}0]$; it is not a screw dislocation and this explains why a slight contrast is still visible in Fig. 6(*a*); $(\mathbf{g},\mathbf{b},\mathbf{l}) \neq 0$ where $\mathbf{l}$ is a unit vector along the dislocation line. Fig. 5 shows the contour map for various values of G; the areas enclosed by the different G values are much smaller than in the preceding case since $\mathbf{g}.\mathbf{b} = 0$. This explains why the complete simulation of Fig. 6(*a*) does not present any dynamical image: there is just a faint intermediary image. If we now set the cut-off value equal to the criterion of the geometrical optics the image obtained, taking into account long-range deformation only ($G \leq 1$), is comparable to the complete one (Fig. 6*b*); the dislocation is not visible in the simulation obtained with $G \geq 1$ (Fig. 6*c*). There is no doubt that curved wavefields explain completely the contrast of this dislocation. The areas where diffraction is predominant are really too small to contribute to the image and the diffracted intensity is negligible.

III. Paths of the wavefields in a plane of incidence

We will now study the paths of the wavefields in the crystal in a setting where the distortion of the crystal may be easily understood. Let us consider an edge dislocation perpendicular to the plane of incidence at half-depth inside the crystal; the extra plane is vertical and on the side of the exit surface of the crystal, which means that $\mathbf{b} = \frac{1}{2}[110]$. The curvature of the net planes corresponds to the curvature of the crystal around the core of the dislocation since the extra plane

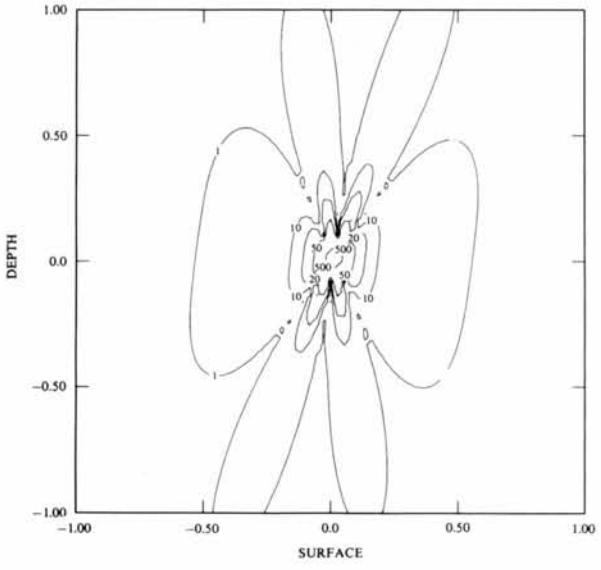

Fig. 5. Contour map for G (same conditions as in Fig. 3, except $\mathbf{b} = \frac{1}{2}[\bar{1}10]$).

is a reflection plane. In a previous study (Epelboin, 1975) we simulated the paths of the wavefields for this geometry but we were unable to distinguish diffraction from geometrical optics. We have repeated the same study for different positions of the dislocation in the Borrmann triangle and for various cut-off values for G. This represents more than 130 different simulations and since they all lead to the same conclusion we present only a few.

(*a*) *Incident plane wave*

Fig. 7 shows the contour map for G; the area is 50 × 50 μm and is larger than in the preceding cases since this dislocation presents a maximum of visibility. Since we now examine wavefields in the crystal Fig. 8 shows their paths in the Borrmann fan in the case of an incident plane wave for which departure from the exact Bragg condition is $\eta = -1$. Fig. 8(*a*) is the simulation with the whole deformation; the succeeding simulations are for $G \geq$ or $\leq n$, where n takes the values shown in Fig. 8(*b*)–(*g*). The refracted beam is on the left and the entrance surface is at the top. Fig. 8(*f*) takes into account areas where $G \geq 500$. It is interesting to note that a narrow beam is still diffracted from the dislocation. This beam is also visible in the complete simulation (Fig. 8*a*) and in all simulations taking into account the most deformed parts of the crystal. It does not appear in Fig. 8(*c*) where $G \leq 10$ and where curved wavefields are predominant; this demonstrates that it is a diffracted wave. Figs. 8(*d*), $G \geq 50$, and 8(*f*), $G \leq 50$, where diffraction is the main phenomenon show great similarities and are not very different from the complete simulation (Fig. 8*a*). This is in agreement with our previous results and shows the importance of diffracted wavefields. Fig. 8(*c*) shows the paths of curved wavefields since $G \leq 10$. We may see how wavefield 1, on the left, is bent by the presence of the dislocation. Fig. 8(*e*) shows the paths when $G \leq 50$. Diffraction and curvature of the wavefields occur together: this image is roughly the superposition of Fig. 8(*c*) where curvature is predominant, and Fig. 8(*f*) where diffraction only exists. We may also notice that the shadow of the dislocation, *i.e.* the dynamical image, does not appear in simulations where geometrical optics are the main phenomena. Moreover, it is not clear from the simulations how the curved wavefields are bent near the core of the dislocation, on account of the local lattice curvature [Fig. 8(*c*) and (*e*)].

(*b*) *Incident spherical wave*

All the features that we have noticed in the case of an incident plane wave are also visible in the case of an incident spherical wave (Fig. 9). We may notice that the shape of the dynamical image is very sensitive to the diffracted wavefields: it is more visible when these are predominant (Fig. 9*b* and *d*) and may not be explained by curved wavefields only. This is also in agreement with the preceding simulations. It demonstrates that diffraction and geometrical optics both contribute to the

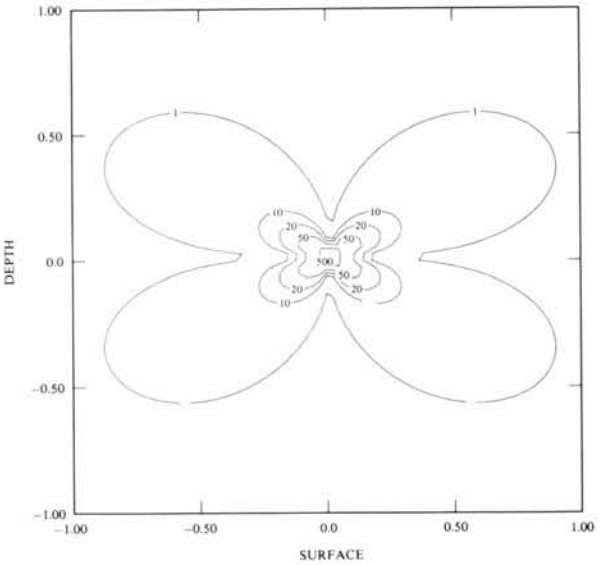

Fig. 7. Contour map for G ($\mathbf{b} = \frac{1}{2}[110]$, Mo $K\alpha$ 220, area 50 × 50 μm).

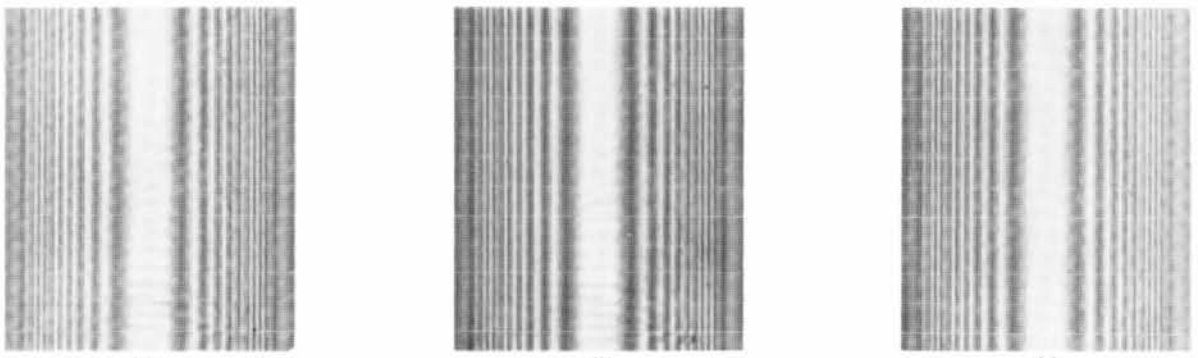

(*a*) (*b*) (*c*)

Fig. 6. Simulated projection topographs (same conditions as in Fig. 5). (*a*) Complete simulation. (*b*) $G \leq 1$. (*c*) $G > 1$.

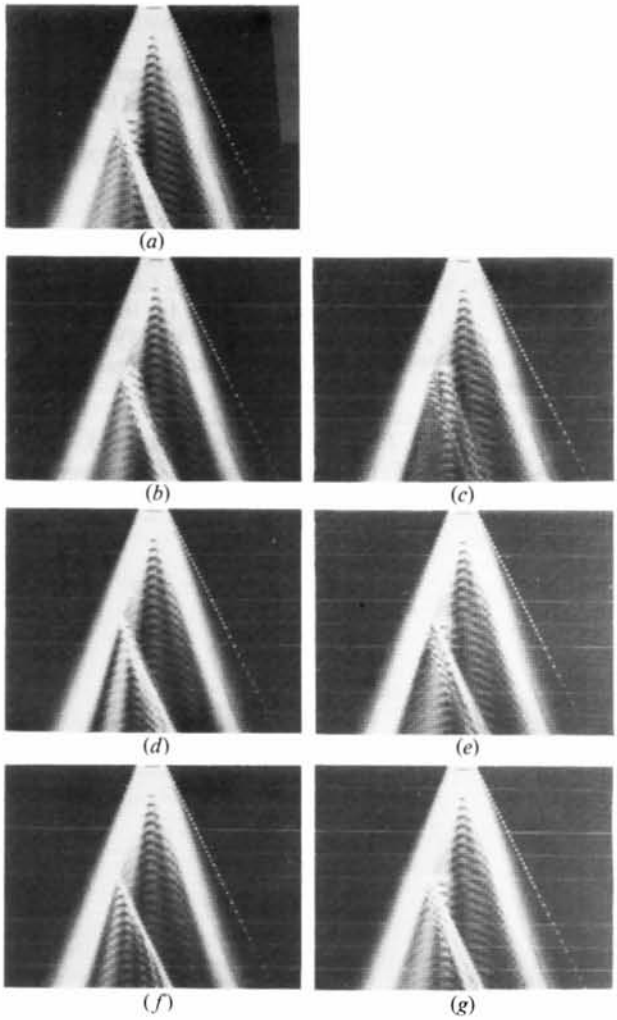

Fig. 8. Paths of the wavefields (conditions as in Fig. 7; incident plane wave, $\eta = -1$; silicon 800 μm thick; position of the dislocation: depth 400 μm, 30 μm on the left of the height of the Borrmann fan). (*a*) Complete simulation. (*b*) $G > 10$. (*c*) $G \leq 10$. (*d*) $G > 50$. (*e*) $G \leq 50$. (*f*) $G > 500$. (*g*) $G \leq 500$.

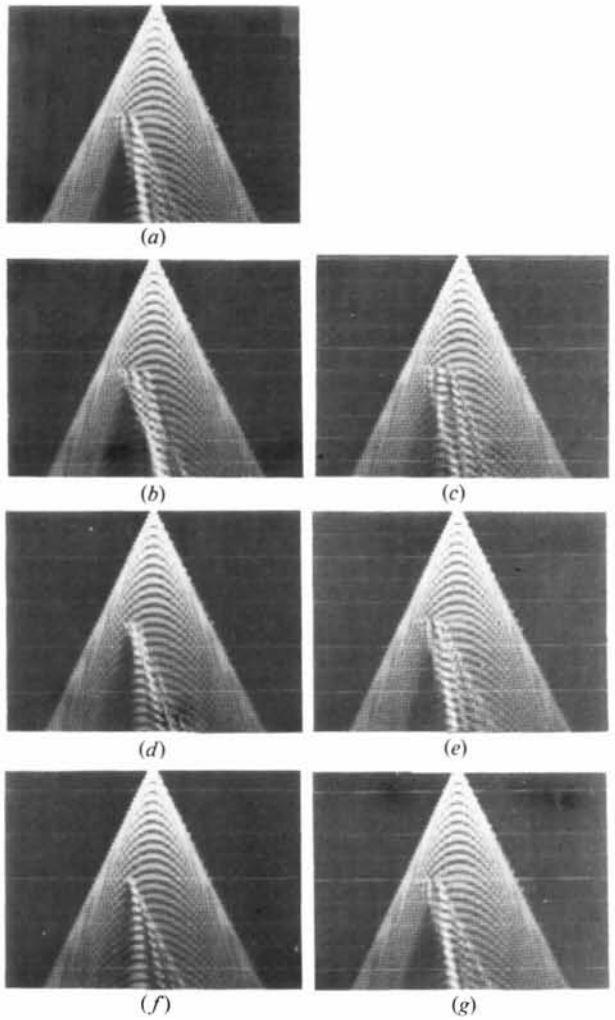

Fig. 9. Same simulations as in Fig. 8 for an incident spherical wave.

formation of the image; there is no doubt that geometrical optics cannot explain such paths for the wavefields near a dislocation and that diffraction is a very important phenomenon.

Simple explanations for the contrast of dislocations should be based on diffraction rather than on geometrical optics and curved wavefields.

Conclusion

For many years it has been well known that diffraction must be taken into account to explain the contrast of dislocations in X-ray topography; we have shown that it is the main phenomenon responsible for the contrast when $\mathbf{g}.\mathbf{b} \neq 0$. However, certain features may be explained by curved wavefields, as, for example, the influence of long-distance stresses to which the dynamical image is sensitive. When a dislocation presents a minimum of contrast, *i.e.* when $\mathbf{g}.\mathbf{b} = 0$, the areas where diffraction is predominant are too small and the contrast may be satisfactorily explained by geometrical optics alone. This may not be true under all conditions and it may happen that, although $\mathbf{g}.\mathbf{b} = 0$, the diffracting volume becomes large enough to contribute to the contrast. Each case must be treated individually. For example, in KDP Balibar & Dunia (1979) have explained by diffraction phenomena the contrast of dislocations presenting a minimum of contrast. It is always desirable to draw the contour map for G in each case.

Many authors have tried to explain the contrast of defects by geometrical optics, using the well known fact that wavefields 1 are bent according to the local curvature of the diffraction planes and wavefields 2 in the opposite direction. From our study it seems that this is too simplistic and it is dangerous to use such explanations, particularly in an attempt to determine

the sense of Burgers vectors. Diffraction effects must be taken into account and the understanding of the contrast of any defect which highly disturbs the crystal may not be reduced to geometrical optics.

This work has been made possible through a fellowship from IBM World Trade.

References

AUTHIER, A. (1967). *Adv. X-ray Anal.* **10**, 9–31.
AUTHIER, A. & BALIBAR, F. (1970). *Acta Cryst.* A**26**, 647–654.
AUTHIER, A., BALIBAR, F. & EPELBOIN, Y. (1970). *Phys. Status Solidi*, **41**, 225–237.
BALIBAR, F. (1975). International Summer School on X-ray Dynamical Theory and Topography, Limoges France, A11.
BALIBAR, F. & AUTHIER, A. (1967). *Phys. Status Solidi*, **21**, 413–422.
BALIBAR, F. & DUNIA, E. (1979). To be published.
BALIBAR, F., EPELBOIN, Y. & MALGRANGE, C. (1975). *Acta Cryst.* A**31**, 836–840.
BALIBAR, F. & MALGRANGE, C. (1975). *Acta Cryst.* A**31**, 425–434.
EPELBOIN, Y. (1974). *J. Appl. Cryst.* **7**, 372–377.
EPELBOIN, Y. (1975). *Acta Cryst.* A**31**, 591–600.
EPELBOIN, Y. (1977). *Acta Cryst.* A**33**, 758–767.
HANDELMANN, S. W. (1975). IBM Res. Rep. RC6005.
KAMBE, K. (1963). *Z. Naturforsch. Teil A*, **18**, 1010–1011.
KATO, N. (1963). *J. Phys. Soc. Jpn*, **18**, 1775–1791.
PENNING, P. & POLDER, D. (1961). *Philips Res. Rep.* **16**, 419–440.
TAKAGI, S. (1962). *Acta Cryst.* **23**, 23–25.
TAKAGI, S. (1969). *J. Phys. Soc. Jpn*, **26**, 1239–1253.
TAUPIN, D. (1964). *Bull. Soc. Fr. Minéral. Cristallogr.* **87**, 469–511.